CEBAF Program Advisory Committee Six (PAC6) Proposal Cover Sheet

This proposal must be received by close of business on April 5, 1993 at:

CEBAF

User Liaison Office

12000 Jefferson Avenue

Newport News, VA 23606

Proposal Title

PRECISION MEASUREMENT OF THE RATIO OF THE ELECTRIC + MAGNETIC FORM FACTORS OF THE NEUTRON WITH POLARIZED ^{3}He USING CLAS

Contact Person

Name: W. HERSMAN

Institution: UNIV OF New Hampshire

Address: DEPT. OF Physics, DEMERITT HALL

Address: Durham, NH 03824-3561

City, State ZIP/Country:

Phone: (603) 862-1950 **FAX:** (603) 862-2998

E-Mail → BITnet: **Internet:**

If this proposal is based on a previously submitted proposal or letter-of-intent, give the number, title and date:

CEBAF Use Only

Receipt Date: 4/5/93 Log Number Assigned: PR 93-037

By: gp

Precision measurement of the ratio of the electric and magnetic form factors of the neutron with polarized ^{3}He using CLAS

V. Boykin, J. Calarco, D. DeAngelis, J. Distelbrink,
L. Gelinas, J. Heisenberg, F. W. Hersman, M. Kennedy,
V. Pomeroy, Timothy P. Smith, I. The, A. Tutein
University of New Hampshire

M. B. Leuschner
Indiana University

V. Burkert, B. A. Mecking, E. Smith
CEBAF

J.-M. Laget
Saclay

and the CLAS Collaboration

F. W. Hersman, Timothy P. Smith, contact persons

ABSTRACT

We propose to measure the polarization response of $^3\overrightarrow{\mathrm{He}}(\vec{e},e'n)$ in the quasielastic region to extract the neutron electric to magnetic form factor ratio (G_E^n/G_M^n) with CLAS. We present a plan to adapt existing techniques for polarizing helium by alkali spin exchange for use in the CLAS. The anticipated precision in the ratio corresponds to an uncertainty of 0.002 in G_E^n at low momentum transfer, and approximately 0.010 at 3 GeV/c^2 (in four-momentum bins of $\Delta Q = 0.2$ GeV/c).

1. Introduction

The neutron electric form factor has been the subject of considerable theoretical and experimental investigation. Because the main component of the nucleon wave function is symmetric, the structure is directly sensitive to small admixtures in the wave function due to color magnetic forces[1] or higher order diagrams in QCD. While the neutron charge radius has been measured by scattering free neutrons from electrons, higher momentum transfer measurements must be performed using lepton beams on neutrons bound in nuclei. Deuterium and ^{3}He are the natural choices. Due to the fundamental importance of neutron properties and the possibility of form factor medium modifications due to binding, measurements from neutrons in both of these nuclei should be performed.

Precision measurements of the deuteron electric form factor have been analyzed in the context of wave functions derived from non-relativistic potential models,[2,3] providing a best fit with a positive value of the form factor, G_E^n around 0.04 in the vicinity of 1.0 GeV/c^2. A Rosenbluth separation of quasielastic electron scattering from deuterium performed recently gave values of $(G_E^n)^2$ consistent with zero. The error bars were also consistent with most credible theories.

Polarization observables enhance the sensitivity to small components of nucleon structure. Polarized ^{3}He provides, to a good approximation, a target of highly polarized neutrons with an almost unpolarized proton background. Coincidence ($\vec{e}$,e'n) measurements can be used to identify the struck nucleon as a neutron, and remove the proton background. The formalism of electron scattering from free neutrons is presented in Chapter 2.

We propose to measure the polarization response of $^3\overrightarrow{\mathrm{He}}(\vec{e},e'n)$ in the quasielastic region. The primary goal of this measurement is to extract the ratio of the neutron electric to magnetic form factor. Measuring the complete angular distribution of the asymmetry provides a measurement of the ratio of G_E^n/G_M^n that is insensitive to the polarization of the beam and target, even insensitive to the fractional polarization of the neutron in the ^{3}He wave function. We propose to measure the angular distribution of the asymmetry for two different beam energies, 1.6 GeV and 3.2 GeV with target angle choices of 40° and 70° that optimize the sensitivity at low momentum transfer and high momentum transfer respectively.

We intend to fabricate a high pressure, polarized ^{3}He target based on the alkali spin exchange technique already in use at several laboratories, adapted for use in the CLAS. The most significant new features of our target are the cylindrical holding field magnet

and a Møller sweeping mini-toroid with low field gradients. Retaining the minitoroid and region one drift chambers allows use of the full luminosity capability of CLAS, and essentially the full resolution capability. The details of the target and its integration in CLAS are presented in Chapter 3.

In Chapter 4 we present the selected kinematics of the quasielastic $^3\vec{\mathrm{He}}(\vec{e},e'n)$ measurements and calculate the counting rates and asymmetries. We explore the possible contamination of the quasielastic process by Δ production and nonresonant processes. Finally we estimate the statistical and systematic precision of the extracted ratio of G_E^n/G_M^n (translated into an uncertainty in G_E^n). We request two weeks for each of the kinematics choices, and one day each for nitrogen subtraction, bringing our total request to 30 days.

2. Quasielastic scattering from a polarized $^3\vec{\mathrm{He}}$ target

The cross section for the inclusive scattering of longitudinally polarized electrons from a polarized target is:[5,6]

$$\frac{d\sigma}{d\Omega d\omega} = \Sigma \pm \Delta(\theta^*, \phi^*)$$

where θ^* and ϕ^* is the spin direction of the target relative to the momentum transfer $\vec{q}$ vector and the plane of the electron scattering. The $\pm$ corresponds to the helicity of the incident electron. The spin independent terms are:

$$\Sigma = 4\pi\sigma_{\mathrm{M}}[v_L R_L + v_T R_T]$$

and the spin dependent terms are:

$$\Delta = -4\pi\sigma_{\mathrm{M}}[\cos\theta^* v_{T'} R'_T + 2\sin\theta^* \cos\phi^* v_{TL'} R'_{TL}]$$

where the response functions depend on the invariant electron variables of momentum transfer Q^2 and energy transfer ω. For the specific case of electrons scattering from polarized (free) neutrons, the spin independent and dependent parts are written:

$$\Sigma = 4\pi\sigma_{\mathrm{M}}[v_L(1+\tau)^2(G_E^n)^2 + 2\tau(1+\tau)v_T(G_M^n)^2]$$

$$\Delta = -4\pi\sigma_{\mathrm{M}}[2\tau(1+\tau)v_{T'}\cos\theta^*(G_M^n)^2 + 2(1+\tau)\sqrt{2\tau(1+\tau)}v_{TL'}\sin\theta^*\cos\phi^* G_M^n G_E^n]$$

A measurement with the momentum transfer $\vec{q}$ direction parallel to the target spin maximizes sensitivity to R'_T, while a measurement with $\vec{q}$ perpendicular to the target

spin accesses the response function R'_{LT}, proportional to G_E^n. It is, however, not the case that the asymmetry is separately sensitive to the magnetic and electric form factors at the different orientations. It can be shown that the asymmetry (Δ/Σ) is sensitive only to the ratio of G_E/G_M by dividing Δ by Σ and factoring out the common $(G_M^n)^2$. The asymmetry is revealed as a function of a single physical quantity, G_E^n/G_M^n and kinematic factors. Setting $\beta = G_E^n/G_M^n$ gives

$$A = \frac{\Delta}{\Sigma} = \frac{2\tau v_{T'} \cos\theta^* + 2\sqrt{2\tau(1+\tau)} v_{TL'} \sin\theta^* \cos\phi^* \beta}{v_L(1+\tau)\beta^2 + 2\tau v_T}$$

Neglecting (for demonstration purposes) the term proportional to β^2, we get:

$$A_{\rm exp} = p_e p_n (k_1 \cos\theta^* + k_2 \sin\theta^* \cos\phi^* \beta)$$

where p_e and p_n are the electron and neutron polarizations and k_1 and k_2 are trivial kinematic factors.

The angular distribution of the asymmetry in the region with the $\vec{q}$ direction perpendicular to the target spin provides a good measure of G_E^n/G_M^n. Location of the kinematics where the asymmetry vanishes, for example, provides maximal sensitivity to G_E^n/G_M^n but with no sensitivity to the beam and target polarization.[7] Conversely the dominant term in the parallel asymmetry depends on kinematic factors and the beam and target polarization, providing a continuous polarization monitor. Our choice of target angles emphasizes determination of the zero asymmetry kinematic region.

3. Experimental Details

3.1 Target

The target technology we have selected for this measurement has been developed over the past 8-10 years by Tim Chupp[8] and collaborators, and used in several measurements at several laboratories. The high density offered by this technology provides the maximum CLAS luminosity at low beam currents, as well as reducing greatly the sensitivity of the polarization to magnetic field gradients. Consequently it is the most appropriate and conservative target choice. Integration of this target into the CLAS is nevertheless a complex issue. We will discuss below several of our considerations.

The ^{3}He target is pressurized to 10 atmospheres of helium, or $2.7\times10^{20}/\mathrm{cm}^3$ over a length of 15 cm, for a total thickness of 20 mg/cm^2 or $4\times10^{21}/\mathrm{cm}^2$. An equal areal thickness is in each beam window, assumed to be 90 μm Corning 1720 glass. A beam current of 30 nA will provide a luminosity of 3×10^{33} electron-nucleon/cm^{2}sec on helium or 1×10^{34} electron-nucleon/cm^{2}sec on the entire target, including windows. Since the target walls and the holding field magnet provide some shielding of the wire chambers, this luminosity is within CLAS design goals.

The ^{3}He target is polarized by optically pumping an alkali metal vapor (rubidium) which spin exchanges with helium. Circularly polarized light of 795 nm can be absorbed by s-shell electrons with the opposite spin, promoting them to the p-shell. Subsequent collisions with helium and nitrogen mix the p-shell polarization and promote nonradiative decays to the ground state, with equal probability for each spin state. The depletion of one spin state leads to accumulation of rubidium atomic polarization. Polarization is transferred to helium nuclei through the hyperfine interaction during collisions.

The design uses two cells, a pumping cell and a target cell. The pumping cell is maintained at elevated temperature, adjusted to control the rubidium vapor pressure. It is located 5 cm off-axis. It must be fully illuminated to maximize the polarization. The target cell is held at a lower temperature to assure that the rubidium plates out on the transfer capillary and does not enter the target cell. (Fig. 1) Target polarization is measured by adiabatic fast passage nuclear magnetic resonance. It is also extracted continuously from the scattering asymmetries.

Coincidence quasielastic scattering from neutrons in 100 torr of nitrogen contributes a 14% dilution over the volume of the cell. Coincidences from scattering off of neutrons in the glass windows can be eliminated by electron track reconstruction. Scattering from nitrogen is measured with an equivalent target of the same geometry (with additional nitrogen) and subtracted. While remaining uncertainties in this dilution contribute to uncertainties in the cross section, they do not contribute to uncertainties in the extracted ratio of electric to magnetic form factor. We continue seeking design possibilities that reduce the window and nitrogen thickness.

3.2 Magnetic fields

A new magnet design is used to define the quantization axis. Two independent coils are wrapped around a watermelon-shaped shell 30 cm diameter and 50 cm long. The first coil of aluminum wire is wound like a solenoid to provide a uniform axial field. A dipolar coil wound in a cosine-theta configuration will provide a uniform field along an axis perpendicular to the beam. By adjusting the current in these two windings, an

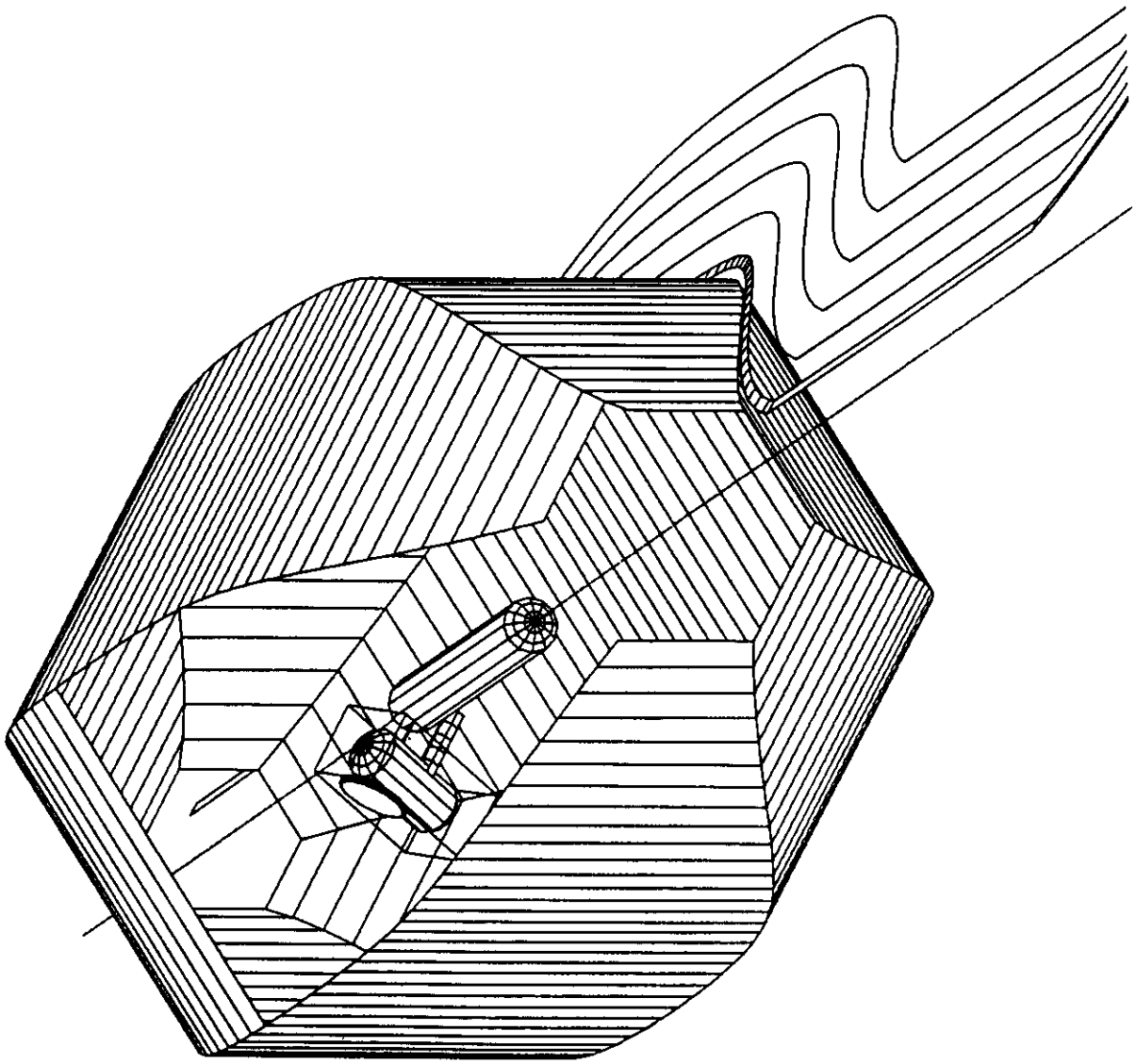

Fig. 1 The alkali spin exchange helium target integrated in the CLAS. The minitoroid coil with its gradient canceling loops, the watermelon holding field magnet, and the two-cell target are indicated. Granularity in surfaces of revolution are an artifact of the drawing program.

arbitrary spin quantization direction can be achieved.

While the goal is to immerse the entire target in a single uniform magnetic field, the magnetic field homogeneity is subject to two distinct constraints. As the helium diffuses throughout the target volume it samples the magnetic field in different regions. Spatial variations of the field appear locally to a moving helium atom as time variations, leading to spin relaxation. The relaxation rate is half the diffusion velocity (D=0.5 cm^2/sec) multiplied by the fractional change in magnetic field per unit length.

$$\Gamma_B = \frac{1}{2} D \frac{(\nabla B_T)^2}{B_0^2}$$

A uniformity of one half percent per centimeter is required to contribute less than 50 hours to the relaxation time (Γ_B^{-1}).

The precision of the data, in particular determination of the asymmetry distribution around the point of zero asymmetry, can be determined with a precision no greater than the knowledge of the quantization axis. This requires that the magnetic field along the beam be uniform and precisely known. This source of systematic uncertainty will be reduced to 4 mrad with a magnet uniformity of one percent. This is the overall design specification for our holding field magnet.

Each coil will be wound with approximately 0.5 mm aluminum wire. The solenoid will have two wrapping layers, while the cosine-theta coil will be accomplished by varying the number of layers from 1 to 4. The total thickness of the conductors is approximately 3 mm. A plastic sheath encloses the water cooling jacket. Scattered electrons and ejected particles pass through the glass walls of the target cell, the aluminum conductors, water jacket and sheath on their path to the region one drift chambers. This additional multiple scattering limits the trajectory reconstruction of low momentum charged particles, but contributes only 2 mr to electrons at 1 GeV/c. The influence on momentum reconstruction is minimal.

In addition to the continuous measure of polarization provided by scattering events, the target polarization will be independently measured by adiabatic fast passage nuclear magnetic resonance. This also allows for fast reversal of the spin. The primary field (B_0) is provided by the coils in the watermelon magnet. We intend to include the drive coils (B_1) in the watermelon magnet as well. Their winding configuration is identical to the primary winding, a solenoid and a cosine-theta coil, providing fields in the same plane (also containing the beam). If they are driven in phase and adjusted at the correct proportion, they produce an oscillating field perpendicular to the primary field. The

pickup coils will be small Helmholtz windings located against the pumping cell, and perpendicular to the plane containing the beam and the spin direction. (Note that a conventional drive coil could also be used, with the drawback that is fixes the target angle, and introduces an obstruction.)

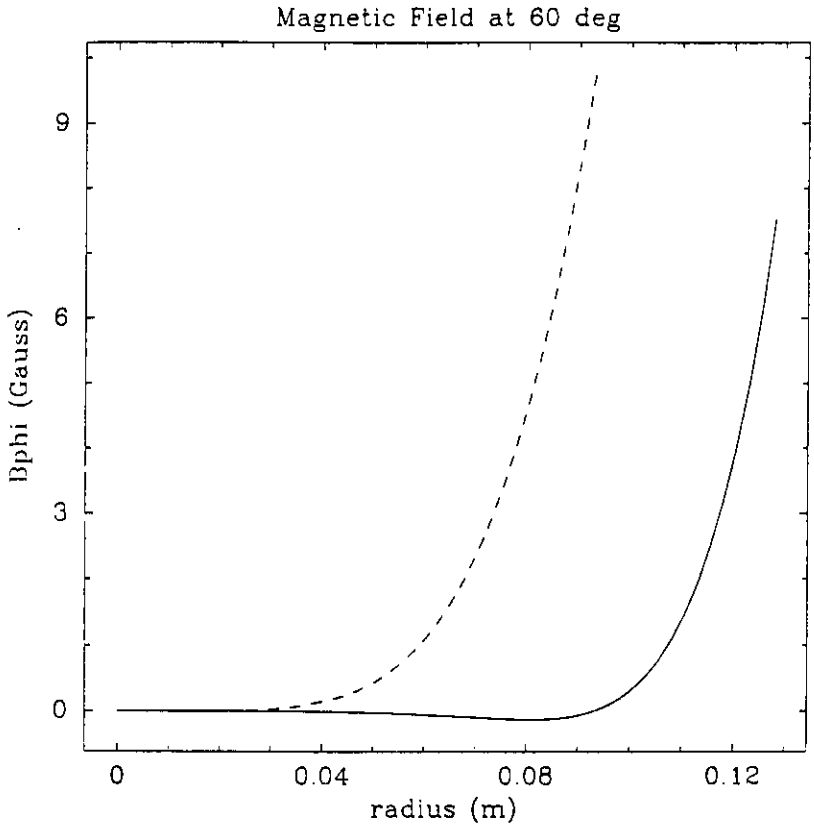

Fig. 2. Azimuthal component of magnetic field at the midplane between coils as a function of radius from the standard target position. Nominal fields rise as the fifth power of the radius. These fields can be canceled by a current in closer proximity flowing in the opposite direction.

This new watermelon magnet does not physically interfere with using the normal configuration of a Møller sweeping minitoroid and the region one drift chamber. (Note that the conventional CLAS first and second level triggers, as well as the standard acquisition and analysis software can also be used without modification.) However, careful attention must be paid to the minitoroid's magnetic field. The minitoroid sweeps Møller electrons from the wire chamber with approximately 200 kA-turns producing 0.1 Tesla fields. These fields leak into the target region leading to off-axis fields that increase as the fifth power of the radius. While these contributions would not effect the precision

of the field at the beam axis, they would reduce the relaxation time. The field B_ϕ reaches 2 gauss at 5 cm, the location of the pumping cell, and rises to 20 gauss at 8 cm (for a nominal coil shape). Increasing the inner diameter of the minitoroid a factor of two (from 17 cm to 34 cm) would reduce these fields by a factor of 32, but eliminate the effectiveness of the Møller sweeping. Instead, the outer windings of the minitoroid can be used for the sweeping field, and the innermost winding be used to contain the leakage fields and cancel the gradients. Approximately 10% of the total current flowing in the opposite direction on the inner winding cancels the gradients (Fig. 2). To achieve the design magnetic field uniformity, this cancellation must be accomplished with an accuracy of 10%. By shimming the spacing between the main loops and the canceling loop the cancellation can be exact. We intend either to influence the design of the minitoroid, or fabricate one meeting our requirements.

Attached to the inner surface of the minitoroid will be one additional conductor, capable of carrying one percent of the total minitoroid current. Six independent power supplies will allow trimming the field for individual coil misplacements.

4. Plan for measurement of G_E^n/G_M^n

We describe our plans to measure quasielastic ^{3}He(e,e'n) to determine the ratio of the neutron electric to magnetic form factor. We choose the coincidence reaction rather than inclusive scattering for the following reasons. By detecting the neutron, we identify the struck nucleon as a neutron, removing the dilution of the asymmetry by scattering from (mostly) unpolarized protons. The enhancement of the asymmetry by a factor of ten improves the statistical figure of merit of the experiment by two orders of magnitude. Larger asymmetries are also less prone to systematic uncertainties. This target technology is less susceptible to depolarization from magnetic field gradients due to its very slow diffusion rates, making it more suited to use inside CLAS. The high density of the target allows beam currents below 30 nA, minimizing depolarization due to ionization and beam magnetic fields. In summary, the conditions for operating this polarized target in CLAS will be very close to the standard operating conditions for electron scattering.

Neutron detection is performed by the electromagnetic calorimeters with efficiency of approximately 40%. A pulse above threshold is required in two crossed elements to localize the point of impact. The forward calorimeters will cover the higher momentum transfer events, while the large angle calorimeter will provide sensitivity to low momentum transfer events. Additionally, neutron measurements of higher precision in energy and coordinates will be provided by the time-of-flight scintillation detectors.

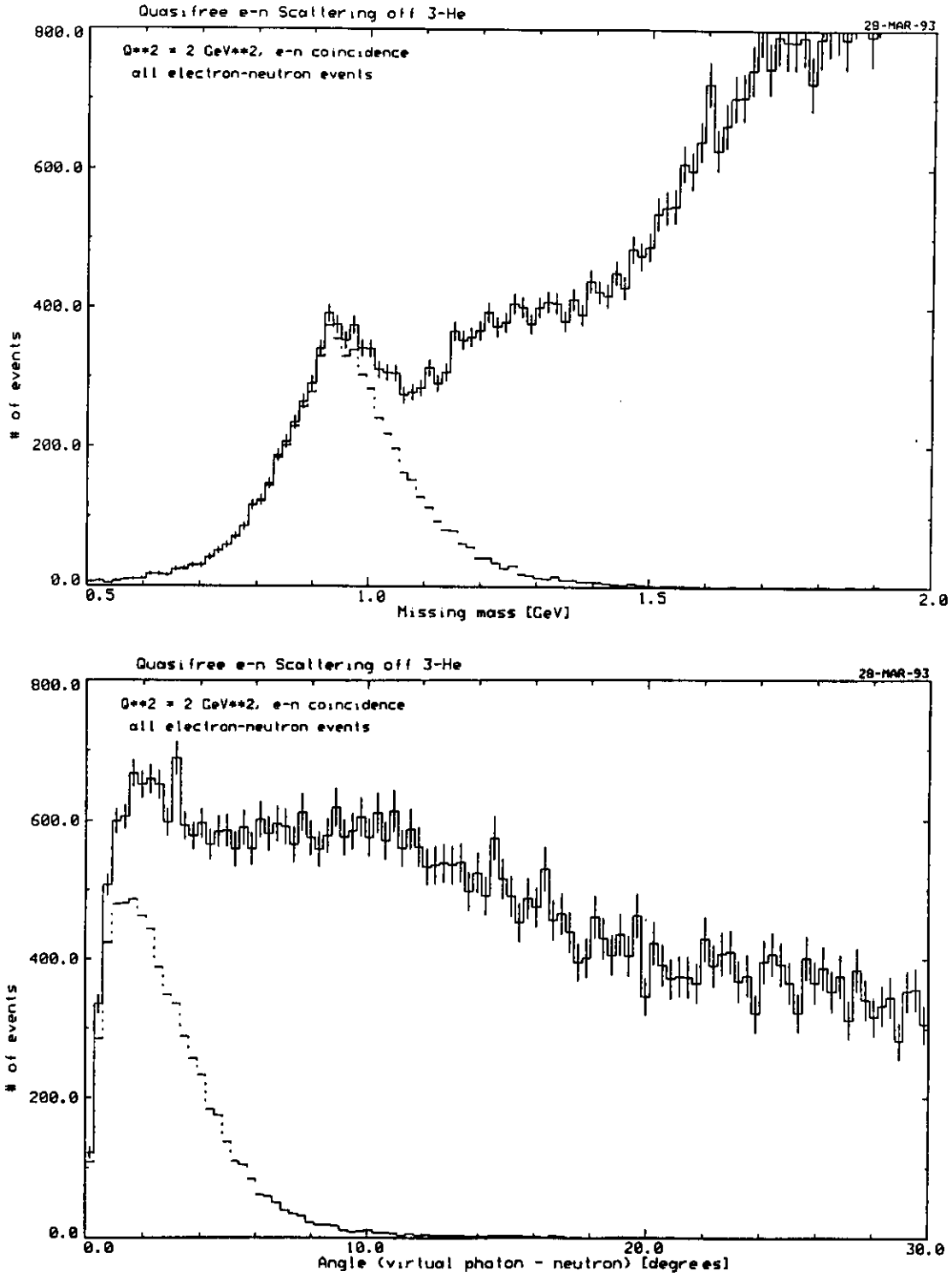

Fig. 3 Quasielastic (e,e'n) events at Q^2=2.0 GeV/c^2 are mixed among the electron kinematics with events from other reaction processes. Most of these events have large neutron angles relative to the momentum transfer.

Theoretical uncertainties, for example two body currents and final state interactions, could limit the precision of the extraction of the neutron electric form factor. Laget has calculated[9] these effects and found them to be negligible above $Q^2 > 0.3$ (GeV/c)^2. Neutrons bound in a nucleus could be subject to form factor modifications of unknown origin. Due to good spatial resolution of the calorimeters, however, we can study the dependence of the extracted neutron form factor on transverse initial momentum. We can also look for variations in the extracted form factor on $x = Q^2/2m\omega$.

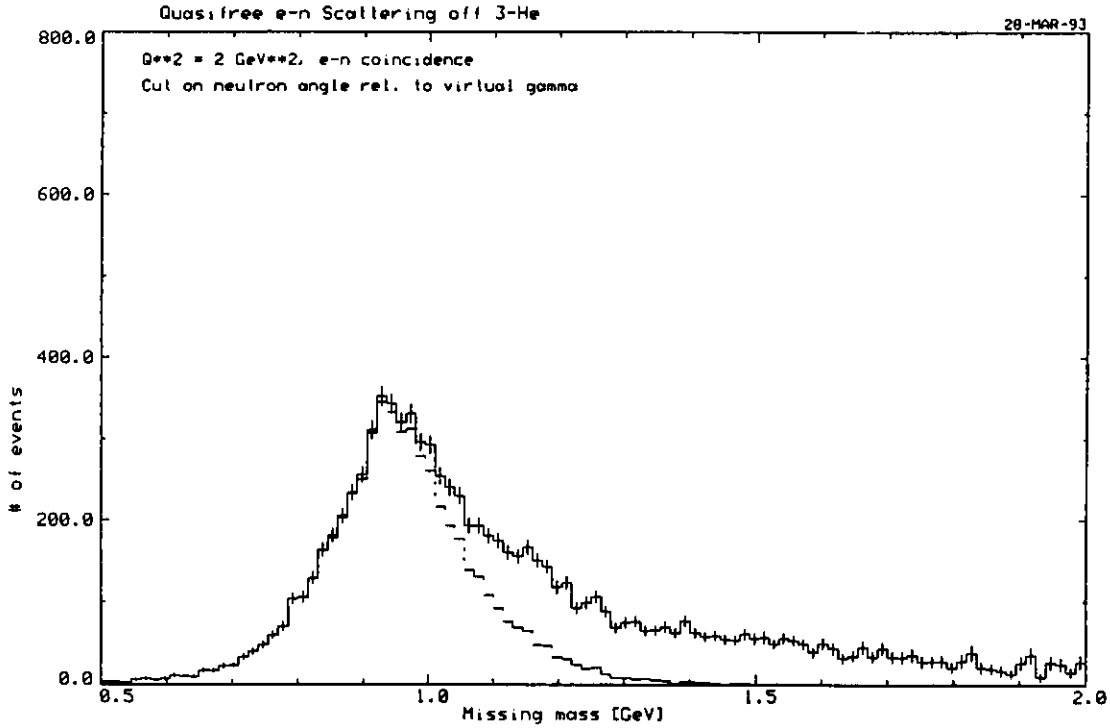

Fig. 4. By performing cuts on the neutron angle, most of the quasielastic events can be cleanly separated. Cuts on both electron and neutron kinematics provide the best filter.

At the highest momentum transfers the Δ production peak and the quasielastic peak merge. Missing energy resolution is not sufficient to discriminate against pion production. Simulations of the contamination of the (e,e'n) quasielastic have been performed taking into account phenomenological descriptions for the quasielastic, Δ, higher resonances, and nonresonant background. As the momentum transfer increases

from 0.5 to 3 GeV/c^2 the contamination of the quasielastic process becomes more significant, particularly on the high energy loss side of the quasielastic peak. Selecting neutrons based on their angle relative to the momentum transfer, i.e. transverse initial momentum, removes most of the other processes. (Figs. 3a,b) These cuts together with cuts in the electron kinematics around $x = 1.0$ select quasielastic events. (Fig. 4) Additional suppression of Δ events can be accomplished by removing events with π^0 photons. The effects of cuts have been included in the uncertainty estimates by reducing the counts at intermediate momentum transfers by 20%, and 40% at the highest Q^2.

4.1 Kinematics

The kinematic parameters that must be chosen for our measurement are the beam energy and the target angle. The goal is to perform precise measurements of the form factor ratio over as large a range of Q^2 as possible. No choice of beam energy and target angle could provide optimal precision over the accessible range. Choosing two beam energies, 1.6 and 3.2 GeV, provides essentially minimum uncertainties with a small (but important) region of overlap. Target angles of 40° and 70° minimize the estimated uncertainty.

4.2 Estimated results

In Figure 5 we show the expected asymmetry for the 3.2 GeV kinematics plotted against laboratory polar and azimuthal angles of the momentum transfer θ_q and ϕ_q. The relative angles θ^* and ϕ^* between q and the target spin direction are superposed. The target direction at $\theta_q = 70°$ and $\phi_q = 0°$ is located at the top and borrom of the graph. Measurements of G_E^n are extracted from events with ϕ_q of 180° near the center of the graph where the asymmetry is small.

TABLE 1a

Counts and asymmetries at $E_0 = 1.6$ GeV and $\theta_T = 40°$

Q	Q^2	counts	Aexp	ΔA	$\partial A/\partial G_E^n$	ΔG_E^n	G_E^n
0.4	0.16	4,880,000	0.021	0.0005	0.27	0.0018	0.029
0.6	0.36	1,790,000	0.009	0.0008	0.41	0.0018	0.044
0.8	0.64	511,000	-.020	0.0014	0.62	0.0023	0.050
1.0	1.0	130,000	-.066	0.0028	0.88	0.0032	0.049

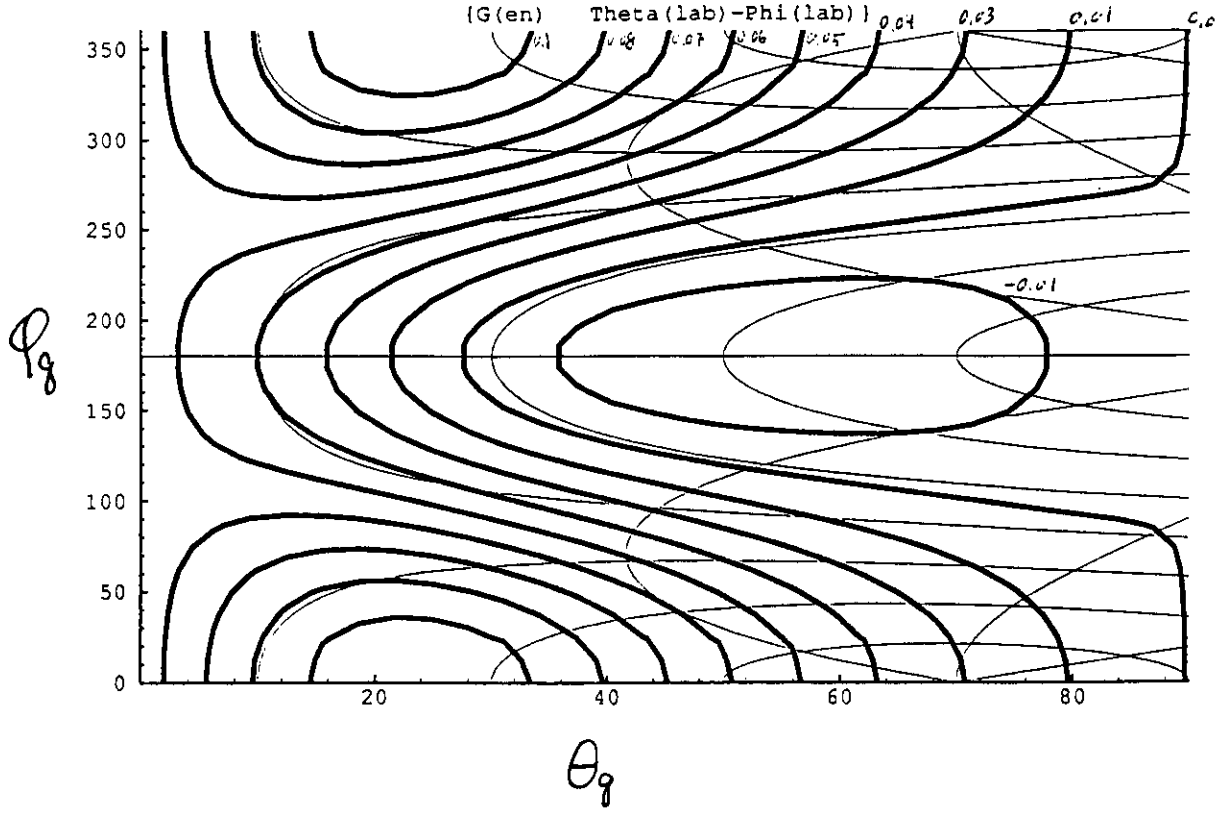

Fig. 5. Kinematics for the measurement at 3.2 GeV. The axes represent laboratory kinematics while the thin contours outline polar and azimuthal angles relative to the target spin direction. The thick lines correspond to contours of the theoretical asymmetry.

TABLE 1b

Counts and asymmetries at $E_0 = 3.2$ GeV and $\theta_T = 70°$

Q	Q^2	counts	Aexp	ΔA	$\partial A/\partial G_E^n$	ΔG_E^n	G_E^n
0.6	0.36	1,069,000	0.036	0.0010	0.18	0.0056	0.044
0.8	0.64	390,000	0.039	0.0016	0.32	0.0050	0.050
1.0	1.0	132,000	0.036	0.0027	0.54	0.0050	0.049
1.2	1.44	43,500	0.025	0.0048	0.87	0.0053	0.045
1.4	1.96	14,000	0.006	0.0084	1.3	0.0062	0.039
1.6	2.56	4,500	-.020	0.0149	1.9	0.0079	0.034
1.8	3.24	1,400	-.053	0.0265	2.5	0.0106	0.030

We present counts, asymmetries, and uncertainties for each of two 14 day runs in Table 1a,b. Only events in one sector of CLAS, the sector with momentum transfer approximately perpendicular to the target spin, were used in the estimates, and were weighted with $\cos\phi^*=1$ (in plane). Azimuthal acceptance varied from 20% at 15° to 80% at 45° and neutron detection efficiency was 40%. The beam polarization was 75% and target polarization was 40%. The estimation was performed for a luminosity of 1×10^{33} on a free neutron. While the quantity extracted from the measurements is the ratio of G_E^n/G_M^n, the uncertainties are represented as uncertainties in G_E^n (with $G_M^n = \mu_n G_D$). Plots of $G_E^n = \tau G_D$ are shown in Figs. 6a,b with our estimates of precision. Final precision is given by the results of the two runs added in quadrature.

4.3 Future work

Two areas where development of the target could result in significant improvement in this measurement are reducing the window thickness and reducing or eliminating the nitrogen quencher. We are pursuing possibilities in these areas. Corning 1720 glass has given long relaxation times for previous targets, so the bulk of the cell will be made from this material. If a proper joint could be formed, then the beam window could be made from another material. A diamond disk 25 μm thick will support 10 atmospheres over a millimeter diameter hole with a good safety margin. The effective luminosity could be tripled with this material. Note that this experiment is not limited by systematics, so the precision of the extracted ratio of G_E^n/G_M^n for a neutron bound in helium would improve by 70%. We will explore grinding a flat surface into the glass to support the diamond, and bonding methods that preserve the high purity of the gases.

Of all the alkali metals and gas quenchers, nitrogen is known to play a special role in quenching rubidium. Unfortunately nitrogen contributes to the scattering. We are analyzing the possibility of using other gases, hydrogen, deuterium, and H-D in particular. Another option would be to freeze out the nitrogen after polarizing the target. While this would reduce the macro-duty-factor of the experiment (one hour polarizing, one hour running), it may enhance the use of the target for simultaneous cross section and asymmetry measurements.

We are developing plans to make full use of all the data provided by this measurement. The (e,e'p) asymmetries provide a measure of the proton S' and D state wave function. The resonance production data, especially the (e,e'π^-p) data, will be used to extract multipole amplitudes. The Δ deformation extending to high momentum transfer would be particularly interesting. We can also extract production amplitudes for the higher mesons, non-strange and strange, from polarized neutrons.

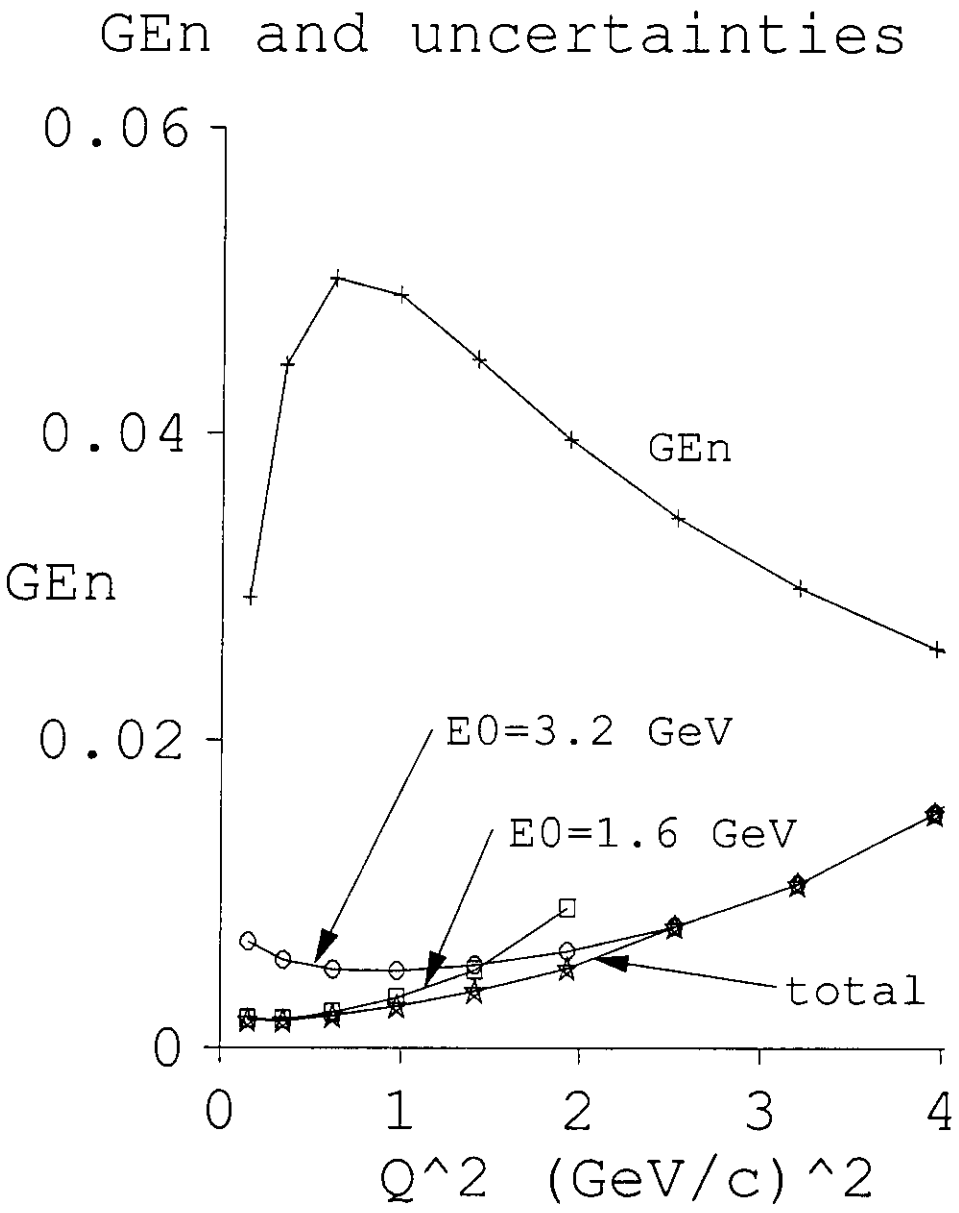

Fig. 6 A model of G_E^n and the estimate of the experimental uncertainty for a 14 day run with one sector of CLAS at incident beam energies of 1.6 and 3.2 GeV.

1. Nathan Isgur, Gabriel Karl, and Roman Koniuk, *Phys. Rev.* **D25** (1992) 25.

2. S. Galster, *et al.*, *Nucl. Phys.* **B32** (1971) 221.

3. S. Platchkov, *et al.*, *Nucl. Phys.* **A510** (1990) 740.

4. A. Lung, *et al.*, *Phys. Rev. Lett.* **70** (1993) 718.

5. B. Blankleider and R. M. Woloshyn, *Phys. Rev.* **C29** (1984) 538.

6. C. Woodward, Ph.D. thesis, Caltech.

7. B. A. Mecking, private communication.

8. T. E. Chupp, *et al.*, *Phys. Rev.* **C45** (1992) 915 and references therein.

9. J. M. Laget, *Phys. Lett.* **B273** (1991) 367.